Check for updates

The mechanism of NOx removal in the sintering process based on source reduction of carbon emissions

Shiwang Han,[a] Ranlei Shao,[a] Luyuan Wang, [ID] *[a] Xingyu Zhang, [ID] [a] Chengbo Xuan,[a] Xingxing Cheng[b] and Zhiqiang Wang[b]

This study systematically investigates the mechanism of NOx emissions during the sintering process, with a focus on the utilization of biochar as an auxiliary fuel to replace a portion of the coke traditionally used in iron ore sintering. The research involved the simulation of sintering raw material ratios using iron ore, biochar, and coke powder. Substitution levels of biochar for coke were set at 0%, 20%, 40%, 50%, 60%, 80%, and 100%. NOx emissions during the sintering process were monitored using a sintering flue gas detection system. Simultaneously, a comprehensive analysis of the sintered ore was conducted with the aim of producing samples that meet sintered ore requirements while reducing NOx emissions. Experimental results revealed that when biomass charcoal substitution for coke reached 50%, the lowest NO emissions were observed during the sintering process, with a reduction of over 90% in accumulated NO emissions in the exhaust gas. In this process, due to the participation of biochar, CO_2 emissions were reduced by approximately 50% compared to traditional sintering processes. The study also analyzed the physicochemical properties of the sintered ore using methods such as XRD, Raman, FTIR, and Vickers hardness testing. The results indicated that the hardness fluctuated within the range of 610 to 710N for sintered products with different levels of biochar substitution, and there were minimal changes in Fe element content and crystal phase transformations.

1. Introduction

China possesses abundant iron ore resources, with an estimated reserve of approximately 20 billion tons, making it one of the world's leading countries in terms of mineral wealth. However, the majority of these resources consist of low-grade ores, and high-grade ores are relatively scarce. Additionally, the complexity of ore types poses challenges for comprehensive utilization. China's iron ore resources struggle to meet the demands of its vast consumption market, and as a result, the country heavily relies on imports.[1] With the rapid development of China's infrastructure and a corresponding increase in steel production capacity, the import volume of iron ore has been steadily rising. Due to various factors, the composition of imported iron ore has undergone significant changes. To achieve a more consistent raw material for blast furnaces, imported iron ore is often blended with domestic low-grade ores and

secondary iron-containing waste materials before undergoing sintering for pelletization.[2] Common methods for pelletizing include sintering and pelletizing. This process consumes a substantial amount of coke fines, constituting a significant energy-consuming step in the steelmaking process. Additionally, it results in the emission of a substantial amount of pollutants, with NOx emissions from the sintering process accounting for 50% of the overall pollution in the steel industry. Therefore, achieving carbon and pollution reduction synergy in the sintering industry is crucial for the low-carbon development of the steel industry. Currently, pollutant emissions from the sintering process mainly include volatile organic compounds (VOCs), nitrogen oxides (NOx), carbon monoxide (CO), and others.[3] Among these, nitrogen oxides (NOx) pose the most significant challenge due to their difficulty in control and high treatment costs, making them a key performance indicator affecting the environmental operation of the sintering industry. NOx control in the sintering process has primarily relied on temperature-based Selective Catalytic Reduction (SCR). However, both the treatment efficiency and catalyst operational lifespan often fall short of ideal levels. In recent years, influenced by the concept of clean production advocated in environmental science and engineering, the approach to achieving "ultra-low emissions" of NOx in the sintering process has shifted from "end-of-pipe control" to "full-process control".[4]

[a]Energy Research Institute of Shandong Academy of Science, Qilu University of Technology (Shandong Academy of Sciences), Jinan, 250014, China. E-mail: hsw550012621@163.com; 2463572722@qq.com; luyuanwang1988@126.com; xyzh@qlu.edu.cn; xcb199602@163.com

[b]National Engineering Lab for Coal-fired Pollutants Emission Reduction, Shandong Provincial Key Lab of Energy Carbon Reduction and Resource Utilization, Shandong University, Jinan, 250061, China. E-mail: 799479710@qq.com; 19862129133@163.com

The sintering process is a crucial component of steel production, wherein the fundamental procedure involves the uniform mixing of powdered iron ore, along with appropriate quantities of fuel and flux, which cannot directly enter the blast furnace. Subsequently, the mixture is ignited and sintered on sintering equipment to produce finished sintered ore blocks. This process aims to enhance the strength and reducibility properties of the sintering raw materials, thereby meeting the requirements for blast furnace smelting.[5] Research has indicated that NO_x generated during the sintering process primarily comprises fuel-type NO_x, along with a minor amount of thermal-type NO_x. Common emission reduction technologies include flue gas recirculation low-nitrogen combustion technology and post-combustion temperature-increasing NH_3-SCR technology. Recent studies have also found that a significant amount of CO in sintering off-gas can serve as a reducing agent, facilitating the conversion of NO_x to N_2 through catalytic action during NH_3-SCR reactions.[6] However, most research focuses on post-generation NO_x reduction, with limited reports on inhibiting NO_x formation during the sintering process. In the sintering process, substituting coke with biomass charcoal not only reduces carbon emissions during sintering but also leverages the complex composition and high alkali metal content of biomass charcoal to lower NO_x generation during combustion, achieving a dual benefit.[7] Liang et al.[8] found that emissions of CO_2 and NO_x are closely related to iron ore mining and sintered ore production. Replacing fossil fuels with renewable energy sources like biomass during iron ore sintering is a crucial approach to reducing carbon emissions in the ironmaking process. Jha et al.[9] used wood chips and charcoal to partially replace coke in sintering and discovered that a 10% substitution with wood chips and a 30% substitution with charcoal produced sintered ore with consistent sintering strength and reducibility parameters. Additionally, due to biomass having nitrogen content 5–10 times lower than coke, it effectively reduces NO_x formation during sintering. Chin-Lu MO et al.[10] explored the impact of carbon and hydrogen-containing chemicals on the sintering process through sintering cup experiments. They found that CH compounds can reduce NO_x emissions by competing with nitrogen for oxygen during heating, thus inhibiting the formation of nitrogen oxides. The addition of biomass increases the porosity of sintering materials and shortens sintering time. Gan et al.[11] circulates the flue gas containing CO into the sintering bed, which can reduce the emission of NO through a reduction reaction. Tsubouchi et al.[12,13] examined the influence of Ca-based additives in sintering materials. Alkaline earth metals and transition metal cations altered the distribution of volatile products during thermal decomposition, subsequently affecting the release of nitrogen-containing products. Their findings suggested that Ca promoted the conversion of N to N_2 under high-temperature conditions, and the presence of CaO catalyzed nitrogen migration.[14] Based on these insights, we propose the substitution of coke fines with biomass charcoal, which contains significant amounts of Na and K elements. While reducing CO_2 emissions, biomass charcoal's low nitrogen and high alkali content, along with the potential catalytic effects of Na and K, can lead to reduced NO_x generation during the sintering process.

This study simulates the sintering process by operating a high-temperature sintering furnace under conditions representative of sintering operations. Iron ore fines, flux materials, coke fines, and poplar wood charcoal are proportionally blended to simulate sintering raw materials, and sintering experiments are conducted at specific temperatures. Real-time collection of off-gas generated during the sintering process is performed, alongside a systematic analysis of the resulting sintered product. In this work, the temporal variation patterns of various components in the sintering off-gas are utilized to deduce the mechanisms of NO_x generation and inhibition. Through characterization techniques such as XRF, XRD, SEM, and FTIR applied to the sintered product, the impact mechanisms of coke fines substitution are investigated. The ultimate aim is to achieve dual objectives of carbon reduction and low nitrogen emissions at the source of the sintering process.

2. Experimental methodology

2.1. Simulation of the sintering process

In this experiment, iron ore particles (mixed with flux), coke fines, and poplar wood were subjected to grinding and sieving processes to obtain particle materials with a particle size of 80 mesh or finer. The iron ore used in this study was sourced from the sintering process of a steel plant in Shandong, China. The coke fines were also obtained from the same steel plant's sintering process, while the poplar wood was purchased from the Lixia Farmers' Market in Jinan, Shandong province, China. The industrial analysis and elemental analysis of these materials are presented in Table 1. Approximately 30 grams of poplar wood particles were carbonized at 600 °C for 2 hours under a nitrogen atmosphere and then naturally cooled to obtain poplar wood charcoal. The iron ore, flux mixture, coke fines, and poplar wood charcoal were placed in a drying oven and maintained at 105 °C for 24 hours to remove surface moisture.

The mixing ratios of iron ore (including flux), coke fines, and poplar wood charcoal were strictly controlled throughout this experiment. According to literature reports, in a conventional sintering process, iron ore (including flux) accounts for 95 wt%, while coke fines account for 5 wt%. Therefore, in our experiment, we maintained this ratio, with the addition of either coke fines or poplar wood charcoal at 5 wt%. We took a 10 g sample of the mixed material, with varying proportions of coke fines and poplar wood charcoal. The poplar wood charcoal substitution levels were set at 0%, 20%, 40%, 50%, 60%, 80%, and 100%, as detailed in Table 2. The sample was sintered in an air atmosphere with a temperature of 1200 °C and a flow rate of 300 ml min^{-1} for 0.5 hours to complete the sintering process of iron ore. After sintering, the sample was transferred to the low-temperature zone, and the hardened sintered ore was cooled to below 50 °C, denoted as A–X. Throughout the sintering process, a gas analysis device (0–2000 ppm NO, 0–10000 ppm CO, 0–25%VOL O_2 intelligent sensor, provided by Xunwei Environmental Protection Co., Ltd) continuously recorded data.

Table 1 Proximate and ultimate analytical results of raw materials[a]

Raw materials	Proximate analysis/%				Elemental analysis/%				
	M_{ad}	A_{ad}	V_{ad}	FC_{ad}	C	H	N	S	O
Coke powder	0.43	21.79	2.68	75.10	74.83	0.25	2.23	1.51	4.11
Biochar	3.09	6.51	12.41	77.99	78.95	1.33	0.42	3.354	13.73

[a] M_{ad}: moisture as received coal; V_{ad}: volatile matter as received coal; A_{ad}: ash as received coal; and FC_{ad}: fixed carbon content.

Table 2 Raw material ratio

	Raw material ratio (wt%)	
Sample	Coke powder	Biochar
A1	100	0
A2	80	20
A3	60	40
A4	50	50
A5	40	60
A6	20	80
A7	0	100

2.2. Characteristics of the sintered ore

The surface morphologies of the samples were observed by field-emission SEM (Tescan MIRA3). The X-ray Fluorescence Spectrometer is tested using PANalytical Axios, which is mainly used to determine the type and content of elements in the material. XRD patterns were recorded on a Smartlab diffractometer using Cu Kα radiation ($\lambda = 1.5056$ Å) at a scanning rate of $5°$ min^{-1} with a step size of $0.02°$ over a 2θ range of $10–90°$. Raman scattering measurements were conducted using a multichannel modular triple Raman system (Thermo DXR2xi, 532 nm, 0.3 mW) with confocal microscopy from 40 to 4000 cm^{-1}. FTIR tests were performed using the Thermo is50/6700 FT-IR Spectrometer. The beam splitter was KBr and the detector was DTGS KBr. The scanning frequency was 32 with resolution of 4 cm^{-1}. The shape, surface characteristics and caking condition of sinter are analyzed. Using the Dutch INNOVATEST FALCON507, ten points were selected for Vickers hardness testing on each sinter sample. The applied load was 100 kgf.

2.3. Assessment of sintering flue gas

A gas pollution detection system, comprised of a high-temperature tube furnace (manufactured by Shandong Wei-kang Scientific Instrument Co., Ltd), gas supply and flow control equipment (float flow meters from Xiangjin Flow Instrument Factory), gas analysis equipment (intelligent sensors covering the range of 0–2000 ppm NO, 0–10000 ppm CO, and 0–25% VOL O_2, provided by Xunwei Environmental Protection Co., Ltd), and a data acquisition system, was employed to study the gas composition generated during the sintering of poplar wood charcoal as a partial substitute for coke fines. Initially, the pollution detection system was purged with 500 ml min^{-1} of N_2 (supplied by Jinan Deyang Special Gas Co.,

Ltd) to reduce experimental errors and remove residual pollutants. Subsequently, during the sintering process of iron ore, continuous airflow at a rate of 300 ml min^{-1} was introduced, directing the sintering off-gas into the detection system. Throughout this period, real-time measurements of NO, CO, and O_2 concentrations in the generated gas were carried out until the completion of the iron ore sintering process, at which point the gas concentrations of NO and CO reached 0, and the O_2 concentration returned to its normal level.

3. Results and analysis

3.1. Apparent observation of sinter

The increasing addition of poplar wood charcoal has a significant impact on the sintering process and the resulting sintered products. As reported,[15,16] during the sintering process, the solid particles in powder form bond with each other, and as the solid grains continue to grow, the porosity of the sintered ore decreases, grain boundaries diminish, and material transfer between particles occurs. This results in an overall volume reduction and an increase in overall density, ultimately producing sintered blocks with a dense polycrystalline microstructure. From Fig. 1, it is evident that as the addition of poplar
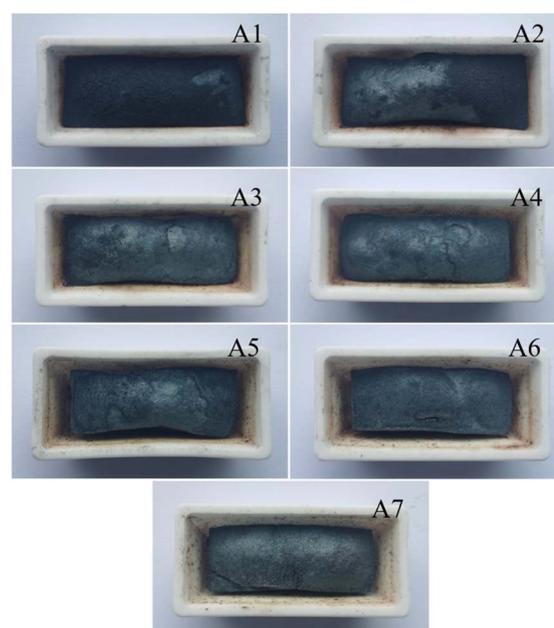

Fig. 1 Photo-graphic images of prepared samples.

wood charcoal increases from 0% to 100%, the surface of the sintered ore becomes smoother, and the volume shrinkage of the sintered ore intensifies. When the addition of poplar wood charcoal is 0%, we can observe a layer of black deposition on the surface of the sintered ore. This is attributed to incomplete combustion during the sintering process. Permeability of sintering raw materials can serve as an important indicator parameter for measuring the sintering process, and the relatively high porosity of biomass charcoal can improve the permeability of sintering raw materials.[17] As the addition of poplar wood charcoal increases, its higher permeability compensates for the unfavorable impact of poor permeability in the sintered ore during iron ore sintering. The iron ore sintering becomes more complete. When the addition of poplar wood charcoal reaches 40%, the deposits generated by incomplete combustion disappear from the sample surface. Beyond a 50% addition of poplar wood charcoal, a significant overall shrinkage phenomenon in the sintered ore becomes noticeable.[18] In summary, the substitution of a portion of coke powder with poplar wood char during the sintering process can expedite sintering by providing heat during the combustion stage. Its inherent characteristics, including low nitrogen content, high oxygen consumption, and promotion of combustion, significantly influence the emission of NO_x during the sintering process.

3.2. Smoke detection and analysis

From Fig. 2, it can be observed that the emissions of NO and CO during the sintering process exhibit a trend of initial decrease followed by an increase as the addition of poplar wood charcoal ranges from 0% to 100%. There are two main reasons for the reduction in NO emissions during the sintering process: during the sintering process, the reaction between the nitrogen (N) in coke fines and oxygen (O_2) generates a substantial amount of fuel-type NO_x. However, as the proportion of added poplar wood charcoal increases, the lower nitrogen content in biomass charcoal leads to a decrease in the proportion of NO_x generated through this process.[19] Additionally, as the biomass charcoal is added, the oxygen consumption increases. Compared to the

traditional process, this results in an overall reducing atmosphere during the sintering process, which is conducive to the reduction of NO_x. Furthermore, the simultaneous decrease in CO and NO levels suggests that CO, released during high-temperature sintering, participates in the reduction of NO through the CO-SNCR reaction, thereby reducing NO_x emissions.[20] During the sintering process of iron ore, when the substitution ratio of biocarbon for coke fines is 50%, the emission of NO during sintering is minimized, with a reduction of over 90% in accumulated NO emissions in the exhaust gas. Chao Liu *et al.*[21] suggested that the optimal addition ratio of biomass charcoal is 40%, under which conditions NO_x is reduced by 25.7%. Regarding the decrease in oxygen content and the increase in oxygen consumption, elemental analysis reveals that poplar wood charcoal has higher fixed carbon and hydrogen content compared to coke fines. This implies that more oxygen is consumed during the reaction process, leading to an increase in CO generation. Fig. 3b shows that sample A4 has the lowest NO and CO content. We speculate that at this particular addition level, the carbon (C) and hydrogen (H) content in the sintering raw materials reaches an optimal value. At this point, the fuel contains a lower nitrogen content, reducing the likelihood of fuel-type NO_x generation. Additionally, during the reaction process, some CO partially inhibits the generation of NO, as previous research has indicated that iron oxide Fe_2O_3 can effectively catalyze the reaction between CO and NO.[22,23] As the content of poplar wood charcoal continues to increase and the oxygen concentration remains relatively low, a significant amount of CH compounds is produced during the sintering process, leading to an increase in instantaneous-type NO_x generation, resulting in elevated NO_x concentrations. Simultaneously, with a lower oxygen content, the combustion of sintering fuel becomes incomplete, causing the CO concentration to decrease initially and then increase with the increasing addition of poplar wood charcoal.
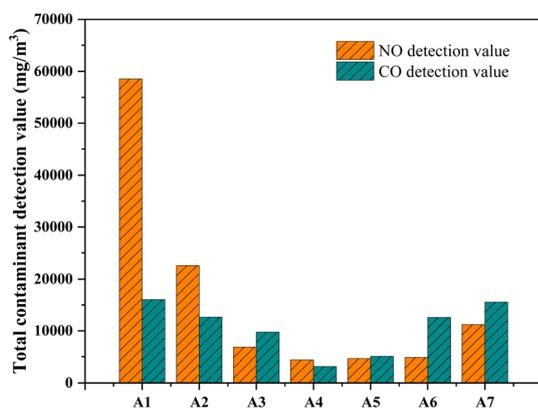

Fig. 2 Total NO and CO emissions in sintering flue gas. Reaction conditions: 300 ml min^{-1} AIR, temperature: 1200 °C.
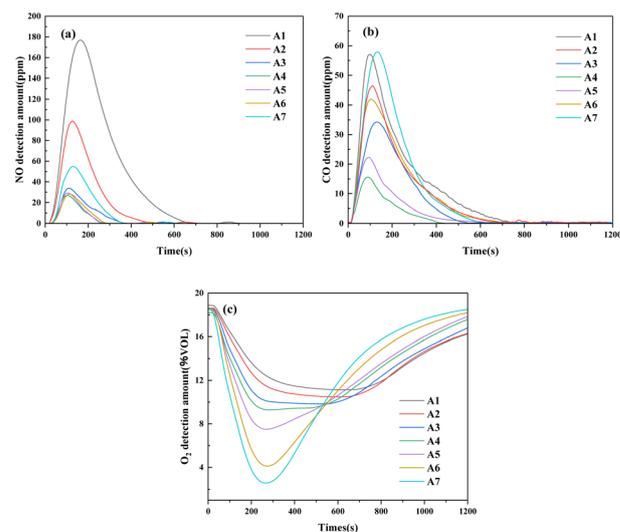

Fig. 3 The detection curves of (a) NO, (b) CO, and (c) O_2 in sintering flue gas. Reaction conditions: 300 ml min^{-1} AIR, temperature: 1200 °C.

From Fig. 3, it can be observed that the release times of NO, CO, and O_2 decrease with increasing poplar wood charcoal addition. In Fig. 3a, it is evident that the NO concentration rapidly increases at the start of the sintering process, reaching a high concentration within 2–3 minutes. Subsequently, after reaching the sintering endpoint, the NO concentration starts to decrease rapidly. The trend in CO concentration mirrors that of NO. The addition of poplar wood charcoal shortens the sintering time compared to sintering with iron ore and coke fines. This suggests that poplar wood charcoal exhibits higher reactivity and lower specific heat capacity compared to coke fines. The reactivity of poplar wood charcoal is attributed to its combined combustion characteristics resulting from its ssurface area and inherent fuel properties. Its relatively high porosity enhances gas permeability, while simultaneously enhancing microscale heat transfer, thus shortening the duration of high-temperature reactions.[24] Yukihiro et al.[25] found that annealing during iron ore sintering reduces NO_x emissions. This suggests that reducing the reaction time at high combustion temperatures can lower NO emissions. The results in Fig. 3c are consistent with elemental and industrial analyses. The increased content of fixed carbon and hydrogen in the sintering process leads to an increased oxygen consumption. Consequently, as poplar wood charcoal is added, the oxygen concentration at the outlet decreases significantly. Comparing CO and NO concentrations, it can be observed that the concentrations of both decrease initially and then increase with the addition of poplar wood charcoal. This is likely due to the combustion process. As poplar wood charcoal is added during the sintering process, the combustion rate accelerates. The depletion of oxygen concentration during combustion on one hand leads to an increase in CH compounds in the sintering process, further promoting the increase in instantaneous-type NO. The generation of instantaneous-type NO_x is accompanied by CO-SNCR. Thus, the increase in NO_x is weaker than the increase in CO. As the sintering process concludes, the O_2 concentration rapidly increases. However, upon comparison, it is evident that the addition of biomass charcoal shortens the entire sintering process, as indicated by the time taken for the oxygen concentration to recover to the inlet concentration. As reported,[10] there is a competitive relationship between hydrogen or carbon in poplar wood charcoal and nitrogen for oxygen in the combustion system. Therefore, the presence of C, CO, H, or OH in the combustion system will inhibit the formation of NO_x. By reducing the availability of oxygen in the sintering system and shortening the duration of high-temperature reactions, we can reduce the formation of nitrogen oxides. In summary, during the sintering process, the replacement of some coke fines with poplar wood charcoal provides heat during the combustion stage, accelerates the sintering process, and significantly impacts the NO_x emissions during the sintering process due to its low nitrogen content, high oxygen consumption, and combustion-promoting characteristics.

3.3. XRF analysis

The sintering mixture is composed of various components, primarily Fe_2O_3, CaO, SiO_2, MgO, Al_2O_3, etc. As indicated in Table 3, the Fe_2O_3 content in the samples remains relatively uniform, with levels exceeding 70%, signifying a high overall iron grade.[26] With the increasing proportion of poplar wood biochar, Fe_2O_3 experiences minor fluctuations within a 3% range, with the A4 sample having the highest Fe_2O_3 content percentage among all samples and the A6 sample registering the lowest. As observed in Fig. 3b, the A4 sample exhibits the lowest CO content, suggesting a lesser reducing atmosphere during the iron ore sintering process, which inhibits the reduction of Fe_2O_3 and results in the highest Fe_2O_3 values in the XRF results. Conversely, the A6 sample experiences a greater presence of reducing gases during sintering, thereby promoting Fe_2O_3 reduction. SiO_2 within the sinter is prone to react with FeO, forming low-melting silicate minerals. The presence of these liquid-phase materials on the sinter surface hinders gas diffusion, reducing permeability and the sinter's reducibility. It also has an impact on sinter hardness.[27] The A4 sample has the lowest SiO_2 content, which is advantageous for gas diffusion and pore formation within the sinter. This results in more complete combustion, reduced Fe_2O_3 reduction, and minimized CO generation. In contrast, the A6 sample exhibits the highest SiO_2 content, leading to increased CO generation and enhanced Fe_2O_3 reduction.[28] MgO is an alkaline oxide that can react with acidic oxides like calcium silicate ($CaSiO_3$) at high temperatures, forming low-melting compounds. Therefore, an appropriate amount of MgO can enhance the sinter's fusibility, facilitating the sintering process.[29] Al_2O_3 and other oxide contents show minimal or no significant trends, and impurity content within the sinter has little impact on sinter quality.

3.4. SEM analysis

To investigate the morphological changes in the sintered ores obtained with varying proportions of biochar involvement in the sintering process, scanning electron microscopy (SEM) was utilized to characterize seven sets of sintered ore samples. As shown in Fig. 4, there exist solid grains of varying sizes in the sintered ore, with many small grains adhering to the surface of larger particles. Most of these adhering particles are smaller than 2 μm, indicating that during the sintering process, iron ore underwent a phase transformation from the solid state to the liquid phase. With an increasing proportion of biochar added

Table 3 Oxide analysis of the sintered ore

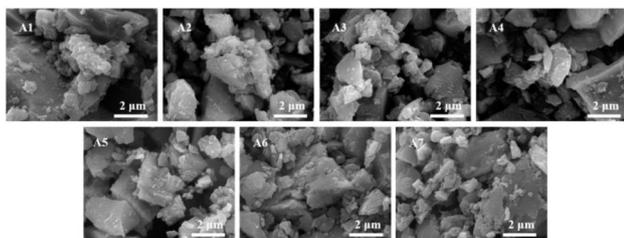| Simple	Fe_2O_3	CaO	SiO_2	MgO	Al_2O_3
A1	74.48	7.43	8.55	7.66	0.69
A2	75.80	7.13	8.07	7.09	0.66
A3	75.65	7.83	7.76	6.88	0.62
A4	76.41	7.01	7.71	7.10	0.57
A5	74.61	7.52	8.24	7.85	0.58
A6	72.19	8.47	8.92	8.66	0.55
A7	75.16	7.03	8.31	7.83	0.52

Fig. 4   SEM images of the sintered ore.

during the sintering process, the distribution of grains in the sintered ore becomes more uniform. Notably, for sintered ores with lower poplar wood biochar content (A1–A4), the structure appears looser, with uneven pore locations and sizes. In contrast, for A5–A7, the pores become smaller, and the structure is more compact. This is attributed to the improved permeability facilitated by biochar, which promotes heat transfer and results in a more even sintering process. Additionally, the combustibility and rapid heat transfer properties of poplar wood biochar contribute to uniform sintering, leading to the formation of more molten phases during the sintering process. Consequently, the porosity and grain boundaries in the sintered ore decrease, enhancing its density.[30] This verifies the conjecture of sinter surface morphology. The microstructure of biochar is relatively loose and there are many pores. During the sintering process, these pores provide more space for the grain growth of sinter and reduce the hardness of sinter to a certain extent.

In order to delve deeper into the influence of nitrogen content in raw materials on NO emissions during iron ore sintering, samples were characterized using Energy Dispersive X-ray Spectroscopy (EDS), as depicted in Fig. 5 This characterization technique provides information about the nitrogen elemental composition in the samples, aiding in our understanding of how nitrogen factors affect the generation and emission of NO during sintering. During the experiment, particular attention was paid to the amount of poplar wood biochar used and its impact on nitrogen content and NO
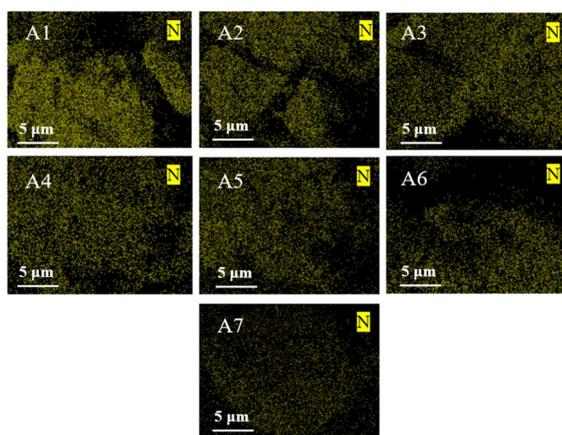
emissions during iron ore sintering. Analysis of the EDS characterization results for samples A1–A7 revealed a clear trend: as the amount of poplar wood biochar used in the samples increased, the nitrogen content in these samples showed a gradual decrease. This finding aligns with the emission curve observed in Section 3.2. In Section 3.2, we meticulously documented the experimental results showing a decrease in NO emissions with increasing biochar content. Combining the results of EDS characterization, we can infer that the addition of biochar may reduce NO generation and emissions during sintering by lowering nitrogen content in the raw materials.

3.5.   Pore structure analysis

From Fig. 6a, it is evident that the studied samples exhibit typical Type III isotherm characteristics. This characteristic is manifested by a concave shape without any apparent inflection points across the entire pressure range. Such a morphology typically signifies that the adsorption process predominantly occurs during the multilayer adsorption stage, wherein adsorbate molecules gradually accumulate on the surface of the adsorbent to form multilayer structures. With an increase in component partial pressure, the quantity of adsorbed gas also rises correspondingly, revealing that the strength of
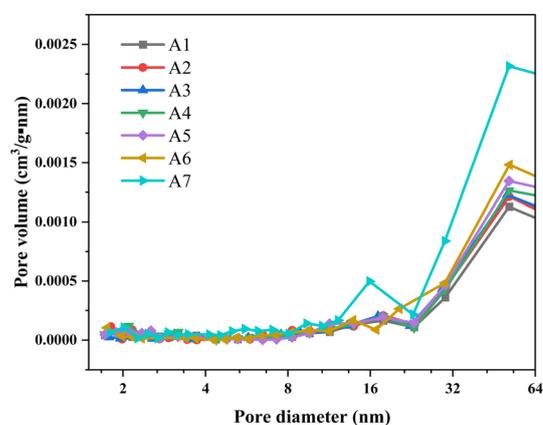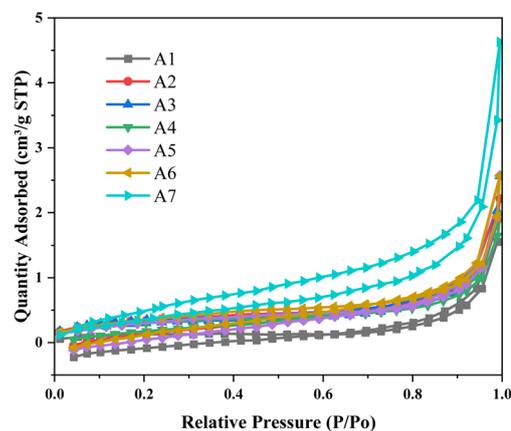

Fig. 5   EDS images of sintered raw materials.

Fig. 6   (a) N$_2$ adsorption–desorption curve and (b) pore size distribution of the sinter.

interactions between adsorbate molecules surpasses that between the adsorbate and the adsorbent. Additionally, the samples exhibit a typical H4 hysteresis loop, indicating the presence of a particular pore structure within the samples.[31] We employed the BJH method to calculate and analyze the pore size distribution, and from Fig. 6b, it can be observed that sample A7 displays the largest pore volume among all tested samples, a result unequivocally confirmed in Table 4. It is noteworthy that poplar wood biochar possesses larger pore volume compared to coke powder, a characteristic that significantly enhances the permeability of raw materials when using a higher proportion of poplar wood biochar in the sintering process of iron ore. Improved permeability facilitates gas diffusion and transport during the sintering process, thereby enhancing the porosity of the sintered ore.[32] The increase in porosity not only improves the physical properties of the sintered ore but also aids in reducing energy consumption and pollutant emissions during the sintering process.

3.6. Hardness testing

Vickers hardness tests were carried out on different sinters. For the same sintering condition, ten points were randomly tested and their average values were taken, and the results were shown in Table 5. It can be observed that when poplar wood biochar is not added, the average hardness of the sintered ore is the highest. However, with an increasing proportion of poplar wood biochar added, there is a trend of decreasing average hardness. The lowest average hardness value is observed for sample A4, which exhibits a hardness reduction of approximately 12% compared to sample A1. This confirms the hypothesis proposed in Section 3.3 that the addition of poplar wood biochar leads to a decrease in sintered ore hardness. The influence on sintered ore hardness involves multiple factors and interactions, with the primary influencing factors being oxide content and sintering conditions. An analysis of oxide content can partly explain the reasons behind these observations. As reported,[32] higher iron oxide content can enhance the hardness of sintered ore. This is because an increase in iron oxide content promotes the formation of a liquid phase during the sintering process, thereby increasing the bonding strength between particles and facilitating the formation of strongly bonded mineral particles, ultimately raising hardness levels, with Vickers hardness values consistently exceeding 600N. SiO_2, as a component of the bonding phase in sintered ore, can cause the appearance of acicular hematite structures in sintered ore when its content is too low, leading to a decrease in sintered ore hardness.[27] Sample A1 has the highest SiO_2 content among all the samples, contributing to its higher hardness. For samples A2, A5–A7, where SiO_2 content varies only slightly, reductions in hardness correspond to decreasing SiO_2 content. Among these, samples

A3 and A4 have relatively lower SiO_2 content, resulting in lower hardness for sample A4. However, sample A3 has a higher CaO content, which favors an increase in sintered ore hardness. An appropriate amount of calcium oxide content can enhance sintered ore hardness by facilitating the formation of a good bonding phase and strengthening the bonding between particles. Excessive calcium oxide content, on the other hand, may lead to over-sintering of the sintered ore and the formation of larger particles.[17] Another factor influencing sintered ore hardness is Al_2O_3, which can promote the formation of a liquid phase during the sintering process and enhance the bonding between particles. However, excessive aluminum oxide content may result in an excessive formation of the liquid phase, weakening the bonding between particles and thereby reducing hardness. In the current experiment, the samples had relatively low and consistent Al_2O_3 content, leading to only a minor impact on sintered ore hardness.[33] The variation in hardness among different sintered ores suggests that with an increasing addition of biochar, more reducing agents participate in reactions, possibly increasing the degree of reduction of oxides in the ore. This, in turn, may lead to phase transformations or the formation of new bonding phases within the sintered ore, resulting in structural and hardness changes. The volatility of poplar coke is a positive factor in creating a reducing atmosphere, helping to reduce nitrogen oxides, unfortunately, its high volatiles hinder the sintering process, because volatiles quickly escape, impeding heat transfer and thermal power, resulting in lower sintering quality, so there is a limit to the amount of coke powder that poplar coke can replace.

3.7. XRD and Raman analysis

Fig. 7a displays the X-ray diffraction (XRD) spectra of the sintered ores. It can be observed that although the characteristic peaks of different sintered ores vary in intensity, they contain essentially the same substances. Fig. 7a reveals that, in addition to SiO_2 and $CaCO_3$, the sintered ores contain a significant amount of iron compounds. The primary forms include FeO (wüstite), Fe_2O_3 (hematite), Fe_3O_4 (magnetite), and $Fe_2(SiO_4)$. The peaks of Fe_2O_3 are more pronounced in A1, A5, A6, and A7, while they are lower in A2–A4. This difference may be attributed to the relatively even distribution of Fe_2O_3 in the sintered ores, with less distinct crystallinity, as well as the occurrence of reduction reactions. The significant presence of Fe_3O_4 in the sintered ores suggests that during the sintering process of samples A1–A7, varying levels of poplar wood biochar addition lead to changes in volatile components in the atmosphere. Additionally, the iron ores undergo magnetic transformations under different atmospheric conditions. In a reducing atmosphere during the sintering process, weakly magnetic minerals like Fe_2O_3 transform into Fe_3O_4, with CO being the primary reducing gas, resulting in higher peak intensities for Fe_3O_4. The appearance of FeO peaks may be attributed to over-reduction during the diffusion of CO to the iron ores, resulting in the formation of wüstite (FeO).[34] The peak strength of SiO_2, MgO and CaO increases with the addition of poplar coke, which is due to the presence of Si, Mg and Ca in poplar coke, while the

Table 4 Textural parameters of samples

Sample	A1	A2	A3	A4	A5	A6	A7
HV (N)	704.45	639	675.59	618.37	624.72	630.65	634.97

Table 5 Sinter hardness test

Sample	Total pore volume (cm³ g⁻¹)	BET surface area (m² g⁻¹)	Adsorption average pore diameter (nm)
A1	0.00026	0.729	25.579
A2	0.00033	0.940	23.694
A3	0.00038	1.077	22.736
A4	0.00042	1.259	17.989
A5	0.00045	1.280	14.293
A6	0.00050	1.570	13.597
A7	0.00051	1.664	11.643
Coke powder	0.005	10.914	6.644
Biochar	0.155	396.303	1.741
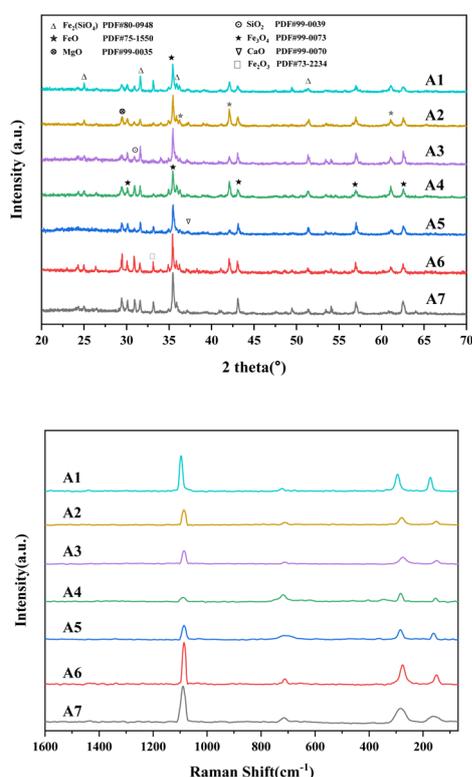
Fig. 7 (a) The XRD spectrum and (b) the Raman spectrum of the sintered ore.

sintering process, signifying structural changes in substances like aluminum oxide (Al_2O_3) and silicate (SiO_2) in the iron ores.[38] The Raman spectroscopy results are consistent with the XRD findings, indicating that during the sintering process of iron ore with partial substitution of coke powder by poplar wood char, the samples contain silicate minerals and hematite phases. Moreover, structural alterations in the iron ore occur during the sintering process.

3.8. FTIR analysis

The FTIR spectra of 7 sinter samples are shown in Fig. 8. It can be seen from the spectra that the functional groups contained in the sinter samples after different treatments are roughly the same. Characteristic peaks at 3686 and 873 cm⁻¹ can be attributed to the O–H stretching vibrations on the surface of hematite.[39] The peak at 1426 cm⁻¹ corresponds to the absorption peak of carbonate, which arises from the vibration of CO_3^{2-} ions. Peaks at 1037 and 945 cm⁻¹ are associated with Si–O vibrations, while the peak at 710 cm⁻¹ represents vibrations in aluminum oxides.[40,41] The presence of peaks at 537 cm⁻¹ (Si–O–Al) and 443 cm⁻¹ (Si–O) is common in hematite and corresponds to lattice vibrations in iron oxides.[42,43] The study indicates that when substituting a portion of coke powder with poplar wood biochar in the sintering of iron ores, the different
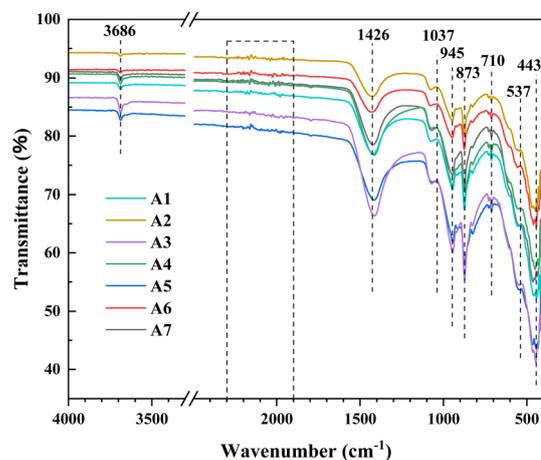
peak strength of $Fe_2(SiO_4)$ in sinter is due to the release of silicon elements in the combustion of poplar coke and coke powder, which may react with Fe_2O_3 in ore. Forming $Fe_2(SiO_4)$ silicate minerals.

To assess the crystalline state of metals in the sintered ores, Raman spectra in Fig. 7b were examined. All samples exhibited four characteristic peaks at 1089, 712, 275, and 150 cm⁻¹. The peak at 1089 cm⁻¹ is attributed to the internal stretching vibration mode of SiO_4 ion groups, indicating the presence of silicate structures in the samples, particularly the tetrahedral SiO_4 structures within the silicates.[35,36] The peaks at 712 and 150 cm⁻¹ are distinctive features of hematite.[36,37] The peak at 275 cm⁻¹ is attributed to the O-T-O bending (T = Al, Si), which results from the rupture of Al–O and Si–O bonds during the

Fig. 8 The FTIR spectrum of the sintered ore.

© 2024 The Author(s). Published by the Royal Society of Chemistry
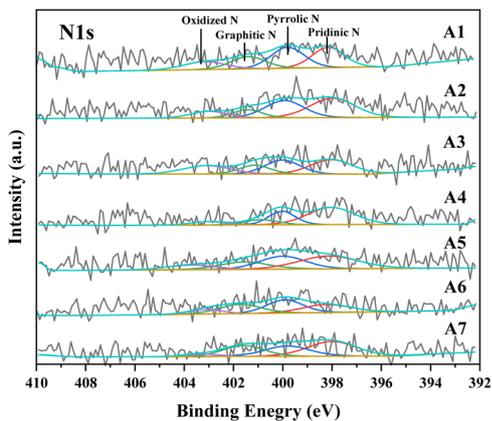
Fig. 9   XPS spectrum of sintered raw materials.

fuel mixture ratios have a minor influence on the functional groups present in the sintered ore. This suggests that the degree of transformation of surface functional groups in the sintered ore is not significantly affected by the amount of poplar wood biochar added.

3.9.   XPS analysis

By employing the Gaussian–Lorentzian method to fit XPS spectra, we can precisely analyze the chemical states of different elements within the samples. In the N 1s XPS spectral analysis of sintered ore samples, we observed diverse forms of nitrogen. As illustrated in Fig. 9, the N 1 s XPS spectrum of the sintered ore exhibits multiple characteristic peaks, whose positions and intensities reveal the various chemical environments of nitrogen within the sample. Further scrutiny of the N 1s XPS spectrum reveals that nitrogen primarily exists in four forms: pyridinic N, pyrrolic N, graphitic N, and oxidized N, located at 398–399 eV, 400–401 eV, 401–402 eV, and 402–405 eV, respectively. Studies indicate the significant role of nitrogen oxides in the generation of NO.[44] By comparing samples with varying poplar wood charcoal content among different sintering raw materials, we observed a decreasing trend in the peak intensity of nitrogen oxides in the XPS spectra as the content of poplar wood charcoal increased, *i.e.*, samples A1–A7. This observation validates the inference made in the testing Section 3.2, suggesting that the addition of poplar wood charcoal can influence the generation of nitrogen oxides during the sintering process.

4.   Conclusion

Utilizing poplar wood biochar with low nitrogen content and zero carbon emissions during the sintering process, it was substituted for a portion of the coke powder traditionally used in the iron ore sintering process to investigate emissions of NO_x and other factors. The results indicated that when biomass charcoal replaced 50% of the coke powder, the NO emissions were minimized. Subsequently, through a series of characterizations, the physical and chemical properties of the sintered ore were systematically studied. Mechanical hardness analysis

was employed to explore the impact of adding biomass on decarbonization, reducing NO_x emissions, and enhancing the quality of the sintered ore. From these investigations, the following conclusions were drawn:

(1) During the sintering process, poplar wood biochar has a higher fixed carbon and hydrogen content. This implies that the addition of poplar wood biochar consumes a significant amount of oxygen during the reaction, creating a reducing atmosphere. Along with the generation of CO, the objective of achieving Selective Non-Catalytic Reduction (SNCR) is attained. Additionally, CO and NO are adsorbed by unsaturated metal active sites on the sintered ore surface, leading to CO-SCR reactions.

(2) During the iron ore sintering process, poplar wood biochar possesses characteristics such as high porosity and excellent permeability, which facilitate efficient heat dissipation, uniform combustion, and accelerated combustion rates within the sintering mixture. This, in turn, reduces the duration of high-temperature reactions and mitigates the formation of NO_x.

(3) Biomass is considered a renewable energy source, and its substitution for coke powder in the sintering process can help reduce the use of non-renewable resources. Additionally, biomass is characterized by its low nitrogen content and zero carbon emissions during combustion, resulting in a significant reduction in NO_x generation and nearly zero net CO_2 emissions into the atmosphere.

(4) The ease of ignition and rapid heat transfer associated with poplar wood biochar result in a more uniform sintering process. During sintering, this promotes the formation of a greater amount of molten material, reduces the voids and grain boundaries in the sintered ore, leading to an increase in its density. However, this increased density may result in a reduction in the material's energy absorption capacity, consequently leading to a decrease in sintered ore hardness.

Author contributions

Luyuan Wang, Xingyu Zhang, Xingxing Cheng, Zhiqiang Wang,: conceptualization, methodology, Shiwang Han, Chengbo Xuan, Ranlei Shao: data curation, writing – original draft preparation, Software, validation. Luyuan Wang: reviewing

Conflicts of interest

All authors declare that no conflict of interest exists.

Acknowledgements

Notes and references

1 R. J. Holmes, Y. Lu and L. Lu, in *Iron Ore*, ed. L. Lu, Woodhead Publishing, 2nd edn, 2022, pp. 1–56.

2 Z. Hao, P. Ma, M. Zhou, Z. Lai and C. Ming, *J. Energy Inst.*, 2018, **92**, S57267803.

3 M. Dai, B. Gu, X. Ma and T. Chun, *Fuel*, 2023, **337**, 127172.

4 L. Cui, K. Ba, F. Li, Q. Wang, Q. Ma, X. Yuan, R. Mu, J. Hong and J. Zuo, *Sci. Total Environ.*, 2020, **725**, 138292.

5 Y. Xu, B. Klein, G. Li and B. Gopaluni, *Miner. Eng.*, 2023, **192**, 108003.

6 M. Gan, Z. Ji, X. Fan, Y. Zhao, X. Chen and Y. Fan, *J. Cleaner Prod.*, 2019, **232**, 1335–1347.

7 S. Zhu, C. Gao, C. Gao, Y. Guo, X. Zhang and X. Li, *J. Cleaner Prod.*, 2022, **373**, 133831.

8 W. Liang, G. Wang, R. Xu, X. Ning, J. Zhang, X. Guo, C. Jiang and C. Wang, *Fuel*, 2023, **345**, 128138.

9 G. Jha, S. Soren and K. Deo Mehta, *Fuel*, 2020, **278**, 118350.

10 C. L. Mo, C. S. Teo, I. Hamilton and J. Morrison, *ISIJ Int.*, 1997, **37**, 350–357.

11 M. Gan, Z. Ji, X. Fan, Y. Zhao, X. Chen and Y. Fan, *J. Cleaner Prod.*, 2019, **232**, 1335–1347.

12 N. Tsubouchi and Y. Ohtsuka, *Fuel*, 2002, **81**(18), 2335–2342.

13 N. Tsubouchi, Y. Ohshima, C. Xu and Y. Ohtsuka, *Energy Fuels*, 2008, **15**, 158–162.

14 H. Suopajärvi, A. Kemppainen, J. Haapakangas and T. Fabritius, *J. Cleaner Prod.*, 2017, **148**, 709–734.

15 C. Chen, L. Lu and K. Jiao, *Minerals*, 2019, **9**, 361.

16 L. Lu and O. Ishiyama, in *Iron Ore*, ed. L. Lu, Woodhead Publishing, 2015, pp. 395–433.

17 C. E. Loo and R. D. Dukino, *Miner. Process. Extr. Metall.*, 2014, **123**, 191–196.

18 J. Wang, H. Meng and H. Zhou, *Fuel Process. Technol.*, 2023, **247**, 107817.

19 N. A. Hayhurst and D. A. Lawrence, *Combust. Flame*, 1997, **110**, 351–365.

20 P. Sun, X. Li, X. Cheng, Z. Wang and P. Wang, *Process Saf. Environ.*, 2023, **176**, 389–401.

21 C. Liu, Y. Kang, Y. Zhang, H. Xing and G. Xue, *Metals*, 2022, **12**, 1483.

22 Z. Gong, W. Wenfei, Z. Zhao and B. Li, *Catal. Today*, 2018, **318**, 59–65.

23 Z. Lei, M. Liu, J. Yan, T. Chun, J. Fang, Z. Li, H. Shui, S. Ren, Z. Wang, X. Cao, Y. Kong and S. Kang, *Fuel*, 2021, **289**, 119779.

24 Z. Cheng, J. Yang, L. Zhou, Y. Liu, Z. Guo and Q. Wang, *Energy Convers. Manage.*, 2016, **125**, 254–263.

25 M. H. Yukihiro, T. Sasaki, Y. Enokido, T. Umezu, S. Iida and Uno, *Tetsu to Hagane*, 1982, **68**, 400–409.

26 Y. U. Zhengwei, L. I. Guanghui, T. Jiang, Y. Zhang, F. Zhou and Z. Peng, *Trans. Iron Steel Inst. Jpn.*, 2015, **55**, 907–909.

27 Z. J. Wang and M. Gan, *Sintering and Pelletizing*, 2014.

28 L. Zhou, Y. Han, W. Li and Y. Zhu, *Sep. Purif. Technol.*, 2021, **276**, 119304.

29 Q. C. Liu, Y. B. Zhang, Y. P. Lan, Q. X. Chen and D. S. Zhang, *Iron Steel*, 2013, **48**, 15–18.

30 J. Wang, H. Meng and H. Zhou, *Fuel Process. Technol.*, 2023, **247**, 107817.

31 J. Wang, H. Meng and H. Zhou, *Fuel Process. Technol.*, 2023, **247**, 107817.

32 Y. Guo, Y. Zheng, Y. Peng, T. Yue and T. Zhu, *Chem. Eng. J.*, 2023, **462**, 142113.

33 Z. Ji, Y. Zhang, M. Gan, X. Fan, X. Chen and X. Huang, *J. Mater. Res. Technol.*, 2020, **9**, 14443–14453.

34 S. Jóźwiak and K. Karczewski, *J. Alloys Compd.*, 2009, **482**, 405–411.

35 D. Wu, H. Huang, M. Ul Haq, L. Zhang, J. Feng and A. Wang, *J. Colloid Interface Sci.*, 2023, **647**, 1–11.

36 N. P. Ivleva, A. Messerer, X. Yang, R. Niessner and U. P Schl, *Environ. Sci. Technol.*, 2007, **41**, 3702–3707.

37 H. Portillo, M. C. Zuluaga, L. A. Ortega, A. Alonso-Olazabal, X. Murelaga and A. Martinez-Salcedo, *Microchem. J.*, 2018, **138**, 246–254.

38 N. Khajehzadeh, O. Haavisto and L. Koresaar, *Miner. Eng.*, 2017, **113**, 83–94.

39 I. Aliatis, E. Lambruschi, L. Mantovani, D. Bersani, S. Andò, G. Diego Gatta, P. Gentile, E. Salvioli-Mariani, M. Prencipe, M. Tribaudino and P. P. Lottici, *J. Raman Spectrosc.*, 2015, **46**, 501–508.

40 W. Salama, M. El Aref and R. Gaupp, *Spectrochim. Acta, Part A*, 2015, **136**, 1816–1826.

41 L. Gong, J. Liang, L. Kong, B. Chen, Y. Li and G. Tian, *Ceram. Int.*, 2021, **47**, 27987–27997.

42 T. C. Ooi, E. Aries, B. C. R. Ewan, D. Thompson, D. R. Anderson, R. Fisher, T. Fray and D. Tognarelli, *Miner. Eng.*, 2008, **21**, 167–177.

43 T. C. Ooi, D. Thompson, D. R. Anderson, R. Fisher, T. Fray and M. Zandi, *Combust. Flame*, 2011, **158**, 979–987.

44 R. K. Vempati, R. H. Loeppert, H. Sittertz-Bhatkar and R. C. Burghardt, *Clays Clay Miner.*, 1990, **38**, 294–298.